Supplementary Material

1. Empirical laws interpolation for the Aegean Sea region

The first thing to do to set up QuakeUp for this event is to interpolate region-specific laws that correlate the PGV and the magnitude to the quantities measured on the P-wave time window chosen. We used seismic events of different magnitudes occurred in the region to calibrate the laws that QuakeUp needs to perform its estimations. The data for this calibration were taken from the accelerometric waveform recorded by the stations in the area during nine events, occurred in the Aegean Sea. The events with their magnitude, location and date of occurrence are listed in Supplementary Table S1.

Supplementary Table S1. In this table we report the origin time, the epicentral location, the hypocentral depth and the magnitude values of the events used to calibrate the empirical laws for the Aegean Sea region.

Origin Time (UTC)	**Latitude (deg)**	**Longitude (deg)**	**Depth (km)**	M_w
2021/08/01 04:31:25	36.3958	27.0112	10.13	5.6
2011/02/28 07:48:52	34.8667	25.4535	54.7	5.7
2020/01/30 11:21:31	35.2254	27.8103	10	5.8
2019/11/27 07:23:42	35.7272	23.2673	71.76	6.0
2011/04/01 13:28:49	35.7317	26.5466	75.5	6.1
2013/06/15 16:11:02.00	34.4507	25.0440	21.5	6.3
2017/07/20 22:30:48.04	36.9249	27.4135	7	6.6
2020/05/02 12:51:06.94	34.2045	25.7124	17	6.6
2014/05/24 09:24:15.62	40.2763	25.3698	8.2	6.9

We didn't use the main event for the calibration of the laws, but we used moderate events with a magnitude range from 5.6 to 6.9. The location and the magnitude of each event were taken from the IRIS Bulletin, where also the recorded waveforms are available [1]. The events were used to interpolate the coefficients for equations 2 (see main text), obtaining the following equations

$$M_w^a = 6.37 + 0.12 \cdot P_a - 0.02 \cdot R \quad SE = 0.5$$

$$M_w^v = 5.56 + 0.45 \cdot P_v + 0.64 \cdot R \quad SE = 0.4$$

$$M_w^d = 5.18 + 0.53 \cdot P_d + 1.69 \cdot R \quad SE = 0.4 \qquad (S1)$$

Where the moment magnitude (M_w^a, M_w^v, M_w^d) is expressed as a function of the logarithm of the hypocentral distance R and the logarithm of the peak in acceleration, velocity and displacement (P_a, P_v and P_d respectively). We notice that the equation for the acceleration parameter has a slightly higher standard error compared to the other two. The magnitude estimated from the acceleration shows also a very low dependence from the distance R compared to the other two magnitude estimations, which is a not very common behavior for such equations. The data and the fitted laws with their uncertainties are reported in figure S1.

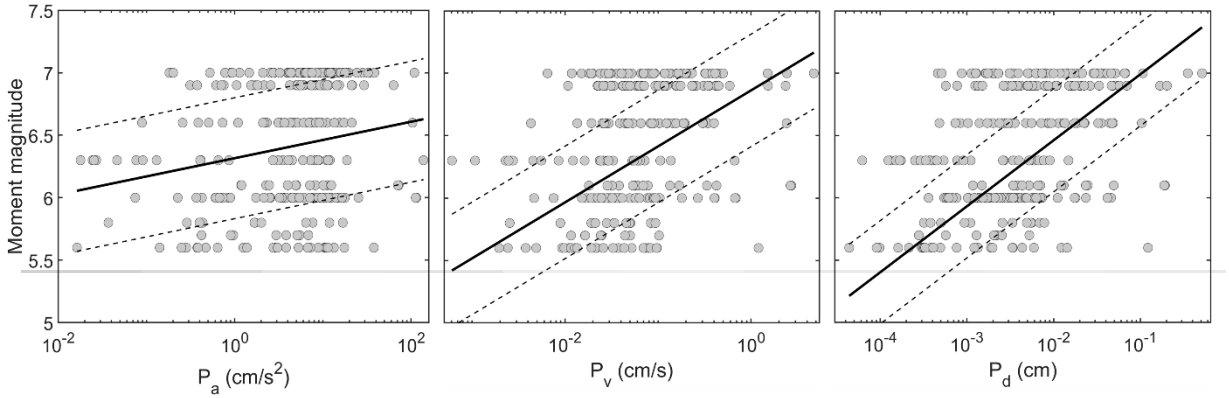

Supplementary Figure S1. Equations S1 are reported visually here (black solid lines) together with their standard errors (dashed lines) and the data used for the calibration (grey dots)

The data from the same events reported in Table S1 were used to interpolate also the relations correlating the PGV to the P-wave amplitudes parameters (equations 1 in the main text) obtaining the following values

$$PGV^a = -0.62 + 0.61 \cdot P_a \quad SE = 0.4$$

$$PGV^v = 0.61 + 0.72 \cdot P_v \quad SE = 0.4$$

$$PGV^d = 0.78 + 0.44 \cdot P_d \quad SE = 0.5$$

(S2)

Where three onsite values of the PGV are obtained as a function of the logarithm of the P wave amplitudes in acceleration (P_a), velocity (P_v) and displacement (P_d). Once again, we notice that the retrieved coefficients for the region are different from the ones obtained for the other two analyzed cases. In Figure S2 we show the obtained laws, and the data used.

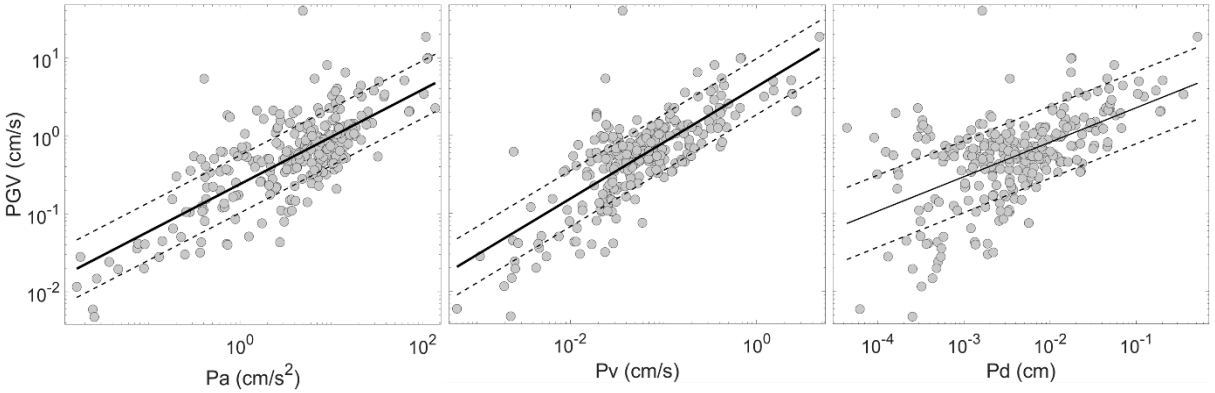

Supplementary Figure S2. The three interpolated laws (black solid lines) are represented with the data used to retrieve them (grey dots). The standard errors of each law are represented as black dashed lines.

Finally, to perform the simulation we set the GMPE for the region, using the laws provided by Akkar and Bommer [2].

2. Empirical laws interpolation for the simulations in the Messina Strait

To simulate a real-time performance of QuakeUp, the attenuation laws for the case must be interpolated. This interpolation is particularly relevant in this case, because we are analyzing simulated events and not real ones. In principle, they should follow attenuation relationships similar to the one calculated on real data, but considering that not all the frequencies are modelled, we can't be sure about that. This is the reason why we interpolated not only the laws involving the P-wave amplitude parameters, but also the GMPE. To do that we used the functional form proposed by Bindi at al. [3] and reported in equation S3

$$Y = e_1 + F_D(R, M) + F_M(M) + F_S + F_{sof} \tag{S3}$$

Where Y can stand for PGA or PGV, but, considering that QuakeUp uses the PGV value for all the prediction, we will use the PGV to interpolate the law. The functions F_D and F_M represent the dependence from the distance and the magnitude. The function F_D is expressed as

$$F_D(R, M) = \left[c_1 + c_2 \cdot \left(M - M_{ref}\right)\right] \cdot \left(\frac{\sqrt{R^2+h^2}}{R_{ref}}\right) - c_3 \cdot (\sqrt{R^2 + h^2} - R_{ref}) \tag{S4}$$

Where R is the epicentral distance, R_{ref} is a reference distance (fixed to 1 kilometre), h is a constant reference depth ($h = 7.9$), M is the magnitude and M_{ref} is a fixed reference magnitude value ($M_{ref} = 5$). The function F_M, instead, is expressed as

$$F_M(M) = \{b_1 \cdot \left(M - M_h\right) + b_2 \cdot \left(M - M_h\right)^2 \quad if\ M \leq M_h \; b_3 \cdot \left(M - M_h\right) \quad otherwise \tag{S5}$$

Where M is the magnitude and M_h is another constant reference magnitude value ($M_h = 6.75$). In equation S3 the term F_S refers to the linear site amplification factor and the term F_{sof} accounts for the faulting style correction. We ignored these two terms in our regression, setting them two zero, since their usage is not implemented yet in QuakeUp. Using the same criteria also the coefficients b_3 and c_3 are set to zero. The coefficient b_3 was originally set to zero by the authors of the GMPE [3]. If we write down the whole equation explicitly, we obtain the functional form that was used in the interpolation procedure

$$PGV = \quad = \{A_1 + A_2(\sqrt{R^2 + 7.9^2}) + A_3(M - 5)(\sqrt{R^2 + 7.9^2}) + A_4(M - 6.75) + A_5(M - 6.75)^2 \quad if \quad (S6)$$

All the coefficients A_n and B_n in equation S6 have been interpolated, obtaining the GMPE used in QuakeUp. An example of these law is shown in Supplementary Figure S3.

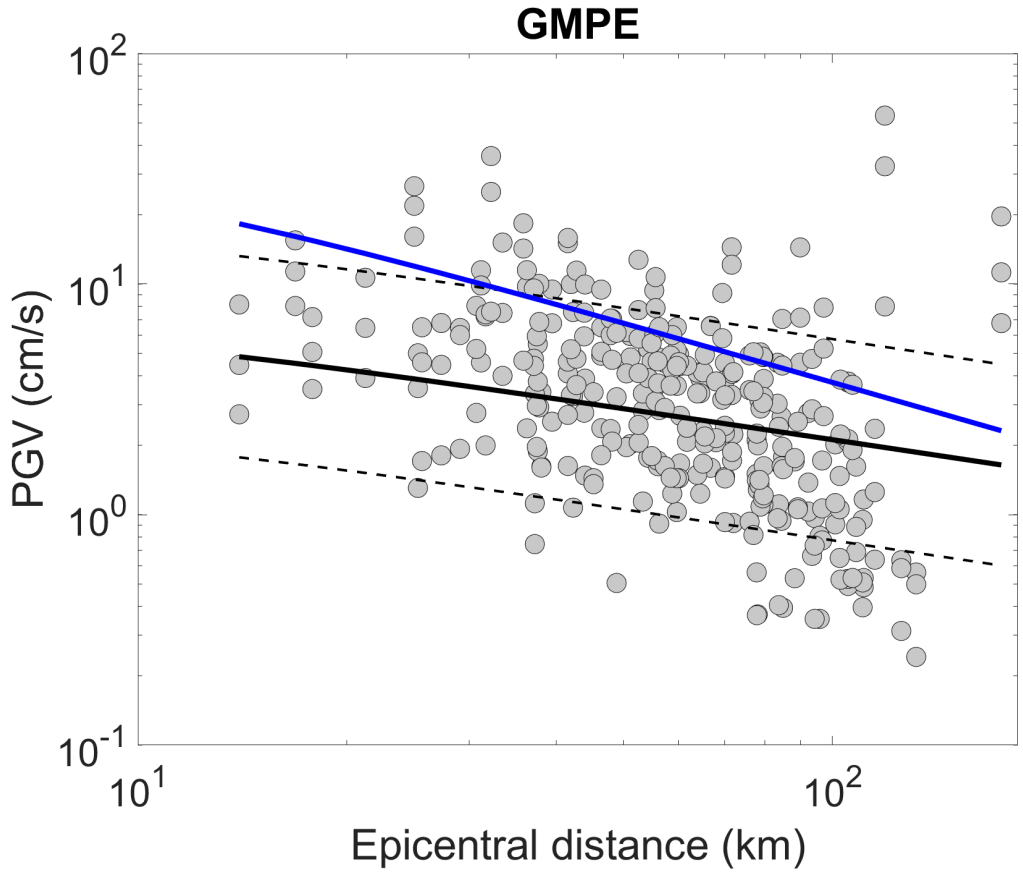

Supplementary Figure S3. The figure shows the interpolated law (black solid line) with its uncertainty boundaries (1 standard deviation, dashed black lines) of three magnitude 7 events simulations. The solid blue line represents the GMPE proposed by Bindi et al. [3] for the same magnitude value. The PGV data at each station for the events are represented as grey dots as a function of the epicentral distance.

In the figure we compare visually the GMPE obtained by us (black line) on the simulated data and the GMPE retrieved by Bindi et al. [3] on real data (blue line). We can immediately notice that the law interpolated on real data would systematically overestimate the simulated values of PGV. To

interpolate all the laws, we used 15 events, corresponding to 1 slip distribution for each magnitude for each epicentral position. This is because the slip distribution shouldn't affect too much the average PGV recorded at the stations. We report all the values obtained in Supplementary Table S2.

Supplementary Table S2. Table reporting all the coefficients values obtained in the interpolation. The coefficients A_n are used for the events with $M \leq 6.75$, while for the magnitude 7 event the coefficients B_n were used

A_1	1.50	B_1	1.23
A_2	-1.05	B_2	-2.02
A_3	0.14	B_3	0.78
A_4	1.38		
A_5	0.43		

Using the same 15 simulated events we calculated also the coefficients for the laws correlating the P wave amplitude parameters to the PGV and the magnitude. To calculate the parameters P_a, P_v and P_d all the traces were manually picked. The time window used for the calculation starts from the P pick and ends at the time of the theoretical arrival time of the S-wave at the station. The interpolated laws correlating the P waves amplitudes to the magnitude have the following form

$$M_w^a = 5.27 + 0.38 \cdot P_a + 0.72 \cdot R \quad SE = 0.3$$

$$M_w^v = 5.62 + 0.31 \cdot P_v + 0.72 \cdot R \quad SE = 0.3$$

$$M_w^d = 5.89 + 0.29 \cdot P_d + 0.69 \cdot R \quad SE = 0.3 \qquad (S7)$$

Here we notice a very strong dependence from the constant value in the equation, meaning that the hypocentral distance R and the P-wave amplitude parameters (P_a, P_v and P_d) count less than the previous cases in the determination of the magnitude. This may be due to the narrow magnitude interval used to produce these laws. It was not possible, however, to extend the magnitude range, because, as we have explained, has an objective difficulty in modelling high frequencies associated with lower magnitude events. The results of this interpolation are shown in Figure 39, where a mean epicentral distance of 30 kilometers to plot equations S7.

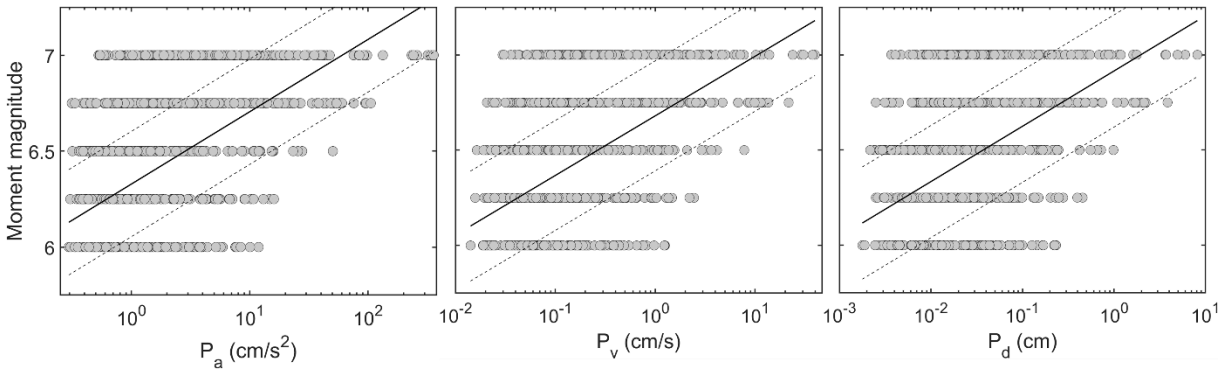

Supplementary Figure S4. This figure shows the interpolated laws correlating the magnitude and the P-wave amplitude parameters. The laws are represented as black solid lines, while their uncertainties are represented as dashed lines. The data used to obtain the laws are plotted as grey dots.

The laws correlating the PGV to the P-wave amplitudes were also interpolated using the usual functional form shown in equation 1 of the main text. The laws obtained are the following

$$PGV^{a} = -0.17 + 0.72 \cdot P_{a} \quad SE = 0.4$$

$$PGV^{v} = 0.51 + 0.61 \cdot P_{v} \quad SE = 0.4$$

$$PGV^{d} = 0.98 + 0.58 \cdot P_{d} \quad SE = 0.4$$

(S8)

Where we notice the same value of the standard error for all the three relations. The relationships retrieved for the synthetic case we set up, do not differ too much from the real cases shown in the previous chapters. This suggests that the case we are simulating is, at least, realistic.

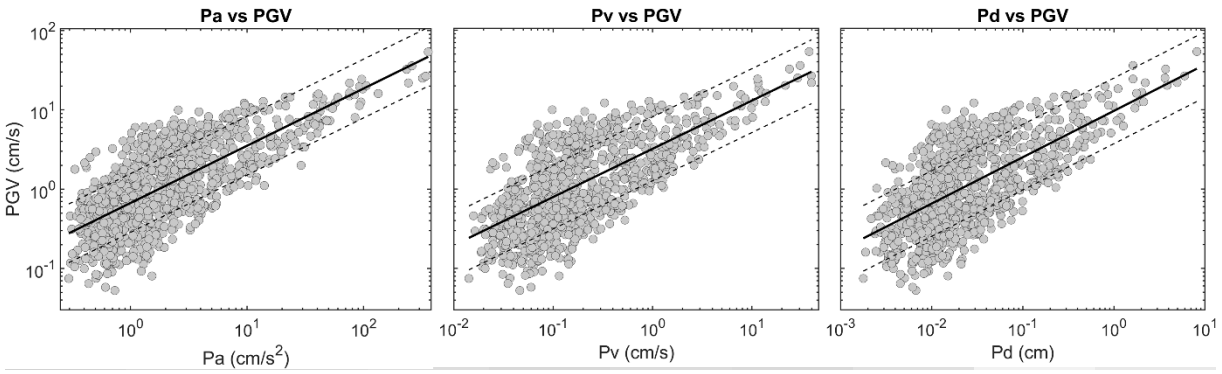

Supplementary Figure S5. Visual representation of equations S8. The black solid lines show the interpolated laws, while the data used for the interpolation are plotted as grey dots. The uncertainty boundaries of the laws are represented as black dashed lines

All these interpolated laws were used to simulate the real-time functioning of QuakeUp on the magnitude 7 event originally associated with the real 1908 Messina event.

3. Statistical study on network reduction performances

To further test the reliability of the method, we simulated 1000 scenarios in which different percentages of the network fail. We simulated a failure of the 30%, the 50% and the 70% of the stations in the network, by randomly choosing the malfunctioning stations for each one of the 1000 scenarios simulated for each percentage. The different network geometries, produced in this way, were used to analyze the performance of QuakeUp on the magnitude 7.0 event. The performances of the system are evaluated by comparing the values of the source parameters estimated by the EEWS and the true value used for the simulation. The time to obtain stable values of these parameters is also calculated in seconds after the Origin Time of the event. Supplementary Figure S6 shows the distributions of the errors in source parameters estimations and the respective

stabilization times. In panel a, we can see that the magnitude is very well estimated by the system, with just one case in which this parameter is underestimated. The average time at which the system obtains a stable value of this parameter is 35 seconds from the origin time (panel d), which is slightly smaller than the one we obtained using the whole network (panel d of figure 5 of the main text). However, it is important to note that the distribution presents two peaks, one around 22 seconds and the other at 38 seconds. This results in a high standard deviation (5 seconds). The peak at 22 seconds may correspond to lucky cases in which the geometry of the reduced network includes the stations closer to the epicenter. The system shows nice performance also in the location

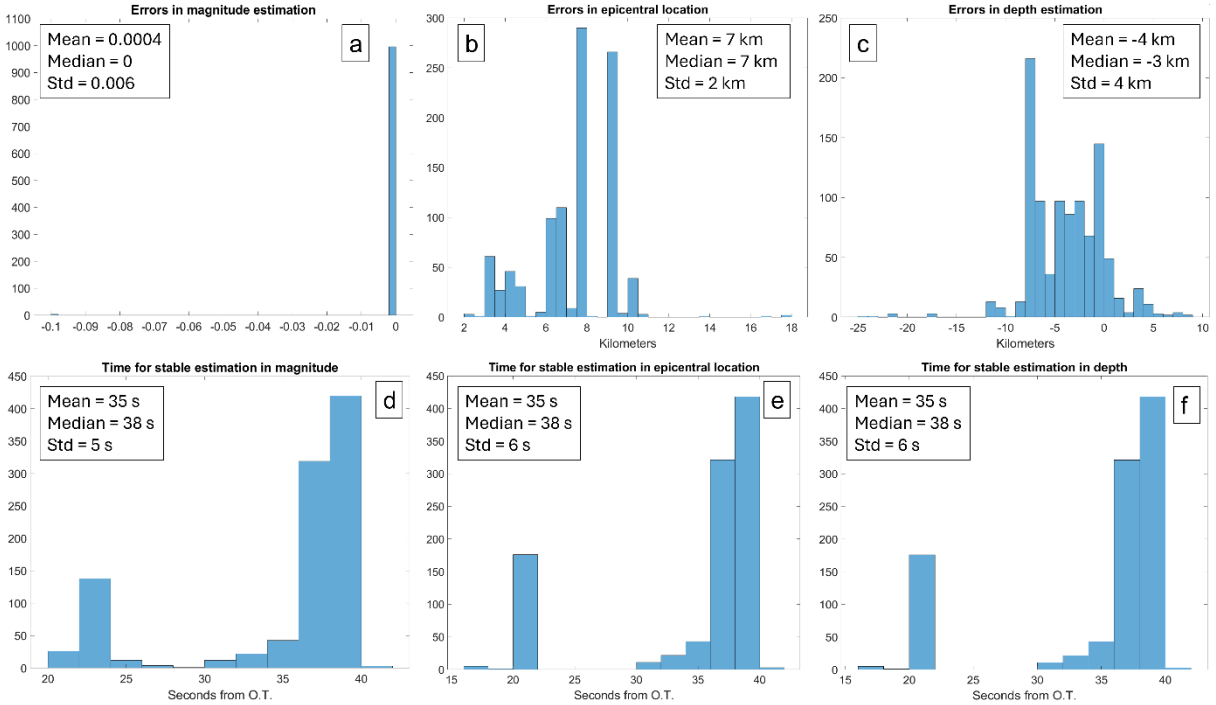

Supplementary Figure S6. In this figure we show the errors in magnitude (panel a), epicentral location (panel b) and depth (panel c) in the estimations obtained by QuakeUp using a network reduced by the 30%. The distribution of the seconds to obtain stable values of these parameters are also shown in panels d, e and f.

estimations, presenting a mean epicentral error of 7 kilometers (panel b) and a mean depth error of -4 kilometers (panel c), indicating a tendency to overestimate the depth value. The distribution of the depth errors has a standard error of 4 kilometers, meaning that it is wider than the distribution of the epicentral distance (with a standard error of 2 kilometers). The time needed to obtain stable values of these parameters presents a distribution shape similar to the magnitude one, with two peaks and an average time of 35 seconds. In these situations, in which the distribution shapes are not gaussian, makes sense to consider the median more than the mean. The median values of all the stabilization time distribution are 38 seconds. It is worth to also look at the uncertainty distributions on the estimations. Looking at figure S7, we see that the mean uncertainty in longitude is 1.3 kilometers and the mean uncertainty in longitude is 4 kilometers. The depth uncertainties distribution shows that the system can be precise in estimating this parameter, having an average uncertainty of 3 kilometers. The problem in the depth estimation is the accuracy, in fact the panel c of figure S6 shows a wide distribution of the errors. Finally, the magnitude is again the best resolved parameter, presenting a median uncertainty value of 0.3.

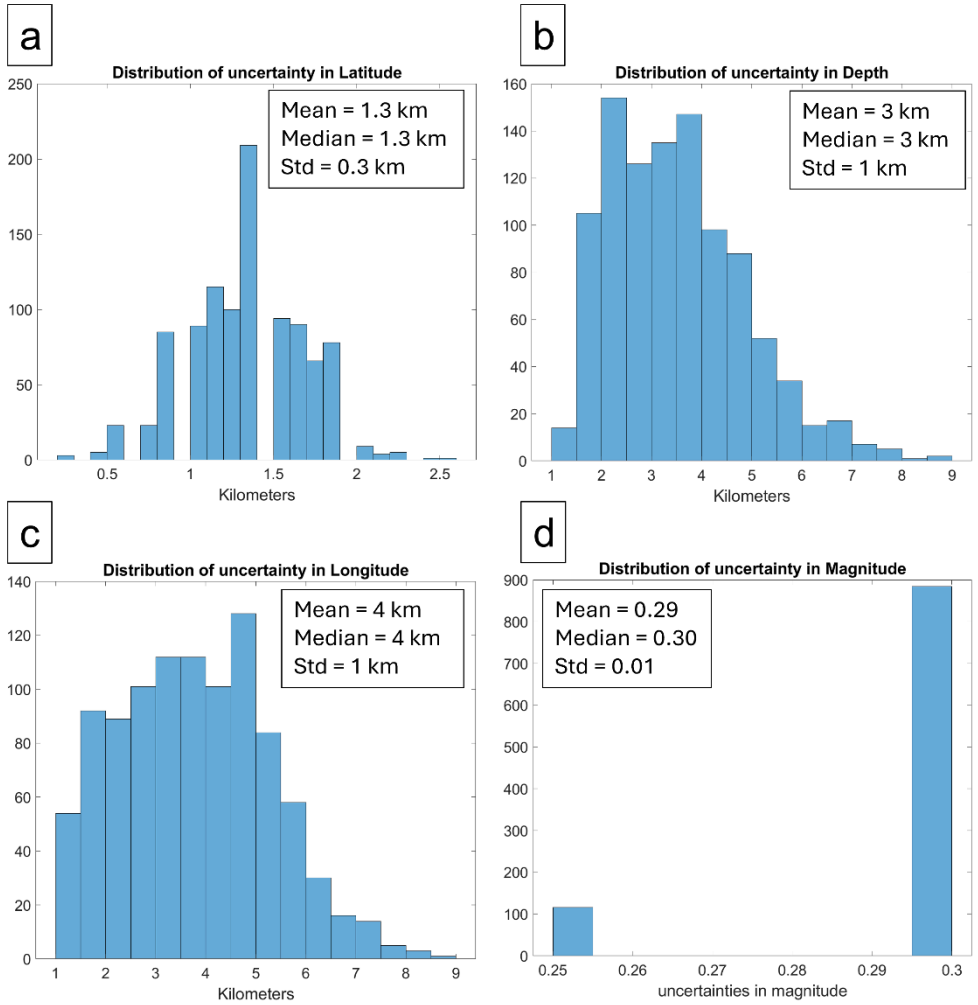

Supplementary Figure S7. The figure shows the uncertainty distributions obtained by QuakeUp for each estimated parameter. The left panels show the uncertainty on the epicentral location parameters, uncertainty in latitude on the upper one (a) and uncertainty in longitude on the bottom one (c). Panel b shows the distribution of the uncertainty in depth and, finally panel d shows the magnitude uncertainties distribution.

The network was further reduced, eliminating the 50% of the stations. The performances on the 1000 scenarios produced with the 50% of the network available are presented in Supplementary Figure S8. It is interesting to note how, again, the magnitude results to be the easiest parameter to estimate correctly, showing 2 cases of underestimation and one case of overestimation (panel a in Supplementary Figure S8). The average values of the location errors are affected by the further reduction operated on the network, presenting higher values than the previous case: 8 kilometers for the epicenter and -4 kilometers for the depth. The distributions of the time needed for the stabilization of each parameter have the same two-peaked shape showed in figure S6. All these distributions have a median value of 38 seconds, but another lower peak is present around 22 seconds. It is interesting to note that the reduced network almost didn't affect these values.

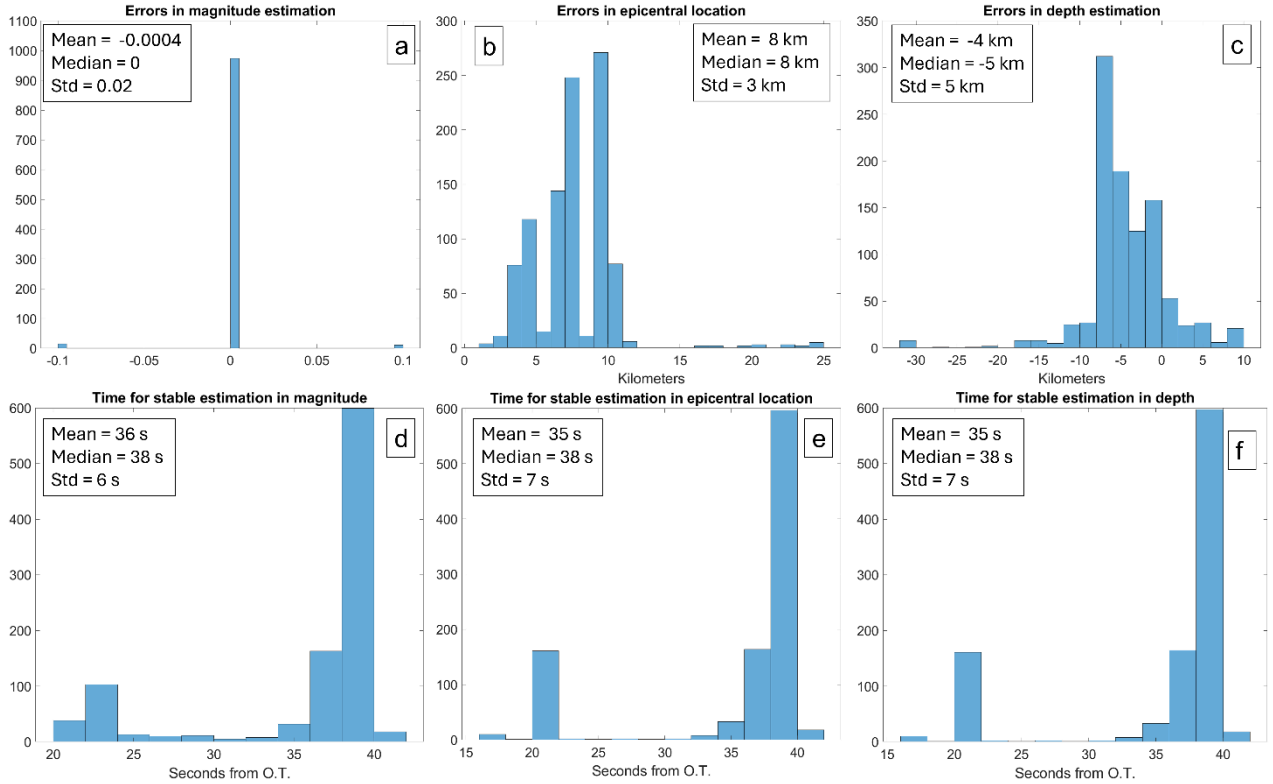

Supplementary Figure S8. Errors distributions obtained by QuakeUp, using the 50% of the network. The distribution of magnitude errors is shown in panel a and the distribution of the time to obtain these values is shown in panel d. Panel b and c show the distribution of the errors in epicentral location and depth value, respectively. The time needed to obtain these values are shown in panel e and f.

The uncertainties obtained by QuakeUp using the 50% of the network are shown in Supplementary Figure S9. As we expected, the average values of the uncertainties of each parameter are higher than the previous case. The mean value of the uncertainty in longitude is 1.6 kilometers and the mean uncertainty in longitude is 4 kilometers, meaning that in this case the method is very stressed and can't be very accurate in epicentral location estimations. The mean uncertainty on the depth is also higher than the previous case, having a mean value of 4 kilometers. This value is still acceptable in the early warning framework, where the quickness of the prediction is more important than the accuracy. The mean value of the magnitude error remains the same as before (0.3), confirming the efficiency of the system in estimating this particular parameter.

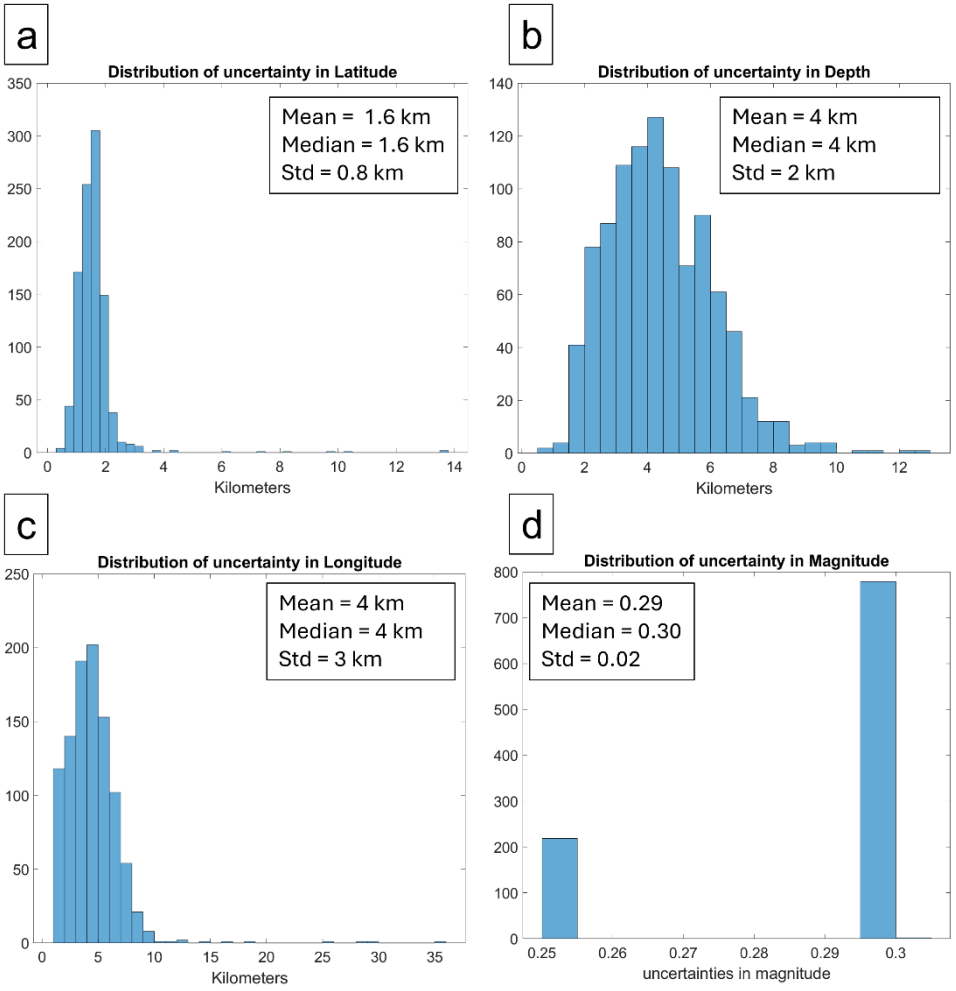

Supplementary Figure S9. The uncertainty distributions obtained by QuakeUp using the 50% of the network are shown here. The uncertainty in longitude (panel c), latitude (panel a), depth (panel b) and magnitude (panel d) are plotted.

To stress more the system, bringing it to its limit we simulated 1000 scenarios in which the 70% of the stations in the network fails. We analyzed the same estimation performances as in the previous cases, obtaining the distribution plotted in Supplementary Figure S10. The magnitude errors distribution, showed in panel a, presents a mean value of almost zero. This value derives from the equal number of overestimations and underestimations and confirms again the great effectiveness of the system in this particular type of estimation. The distribution of the epicentral errors, showed in panel b, have a peak around 7 kilometers, but it starts to show a second low peak at 23 kilometers, meaning that the system is really stressed by this poor network. The average value is, however, 9 kilometers, which is still very useful in early warning framework, for both seismic and tsunami warning. The distibution of the depth errors, showed in panel c, confirms the tendecy of the system in overestimating the value of this parameter, showing a mean value of -5 kilometres. This parameter is very relevant in Tsunami Early Warning, therefore, the fact that QuakeUp can retrive a reliable value of the depth even if the network is largely not working, is very encouraging. The distribution of the times needed to have stable paramters estimations, show again the two-peaked shape that we discussed in the previous cases. In fact, we can see in panels d, e and f that the distributions have a low peak around 22 seconds and a main peak around 39 seconds. The median values of these distributions are in fact exactly 39 seconds, which is higher than the previous case. We expected that the method would be really stressed in this situation and so we expected an higher

average value of the stabilization time. However, it is worth to note that the time needed to have stable source estimations is absolutely in the range usually discussed in early warning framework.

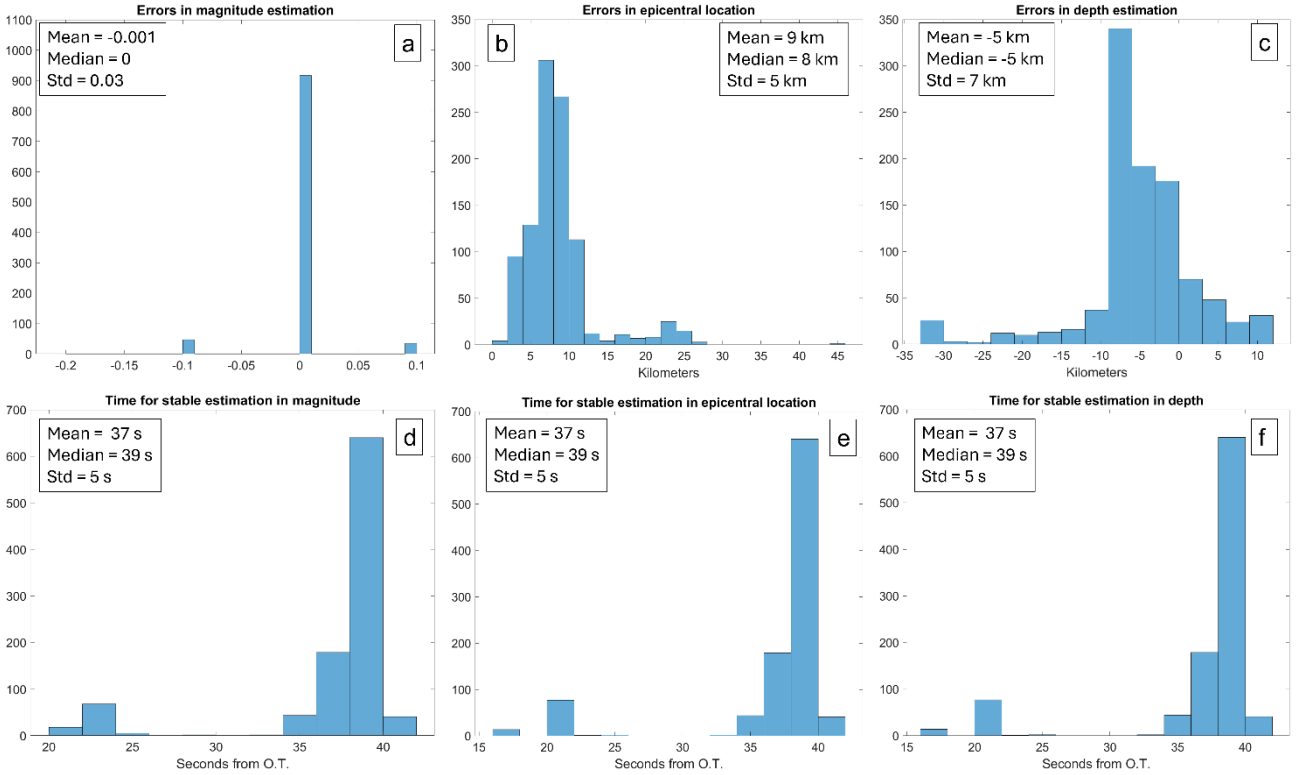

Supplementary Figure S10. In panel a we show the errors in magnitude, calculated as the difference between the estimation and the true value, obtaining a value of zero in most cases. In panel b the epicentral errors distribution is shown, obtaining a mean value of 8 kilometres of epicentral distance. In panel c we show the depth estimation errors calculated as the difference between the true value and the estimated ones, obtaining an average value of -5 kilometres, underlying the tendency of the system in overestimating this parameter. In panels d, e and f we show the distribution of the times needed to obtain stable values of magnitude, epicentral location and depth, respectively.

Also in this case, we present the uncertainty on the estimated parameters provided by the system. As we expected, the network reduction largely affects these uncertainties, as we can see in Supplementary Figure S11. In panel a, the distribution of the uncertainties in latitude is shown. The distribution appears to be well peaked around the mean value of 2 kilometers, but it has some vary high value. In those situations, the system basically can't have a reliable source latitude estimation. A similar shape can be recognized looking at the longitude uncertainty distribution, in panel c. This parameter seems to be less resolved than the others, having a mean uncertainty value of 5 kilometers and showing in the distribution uncertainty values up to 60 kilometers. Such a high uncertainty means that the epicentral location can't be used even in the early warning framework. The depth uncertainties distribution, instead, is centered around the mean value of 5 kilometers. In this distribution there are also values of uncertainty too high to be used effectively in the tsunami early warning framework, in fact in the tail of the distribution there are values up to 13 kilometers (panel b). Finally, the magnitude uncertainties distribution is shown in panel d. The mean value of the distribution is 0.3, exactly the same of the cases analyzed before. This means that the magnitude is very well resolved even if the network is strongly reduced. This is probably because the method uses the independent estimations of the magnitude at the stations to obtain a global value as a

weighted mean (see Method in the main text). This means that even if few stations are working in the area, if they have the right relation to correlate their measurements to the magnitude, they can still retrieve the right value of this parameter.

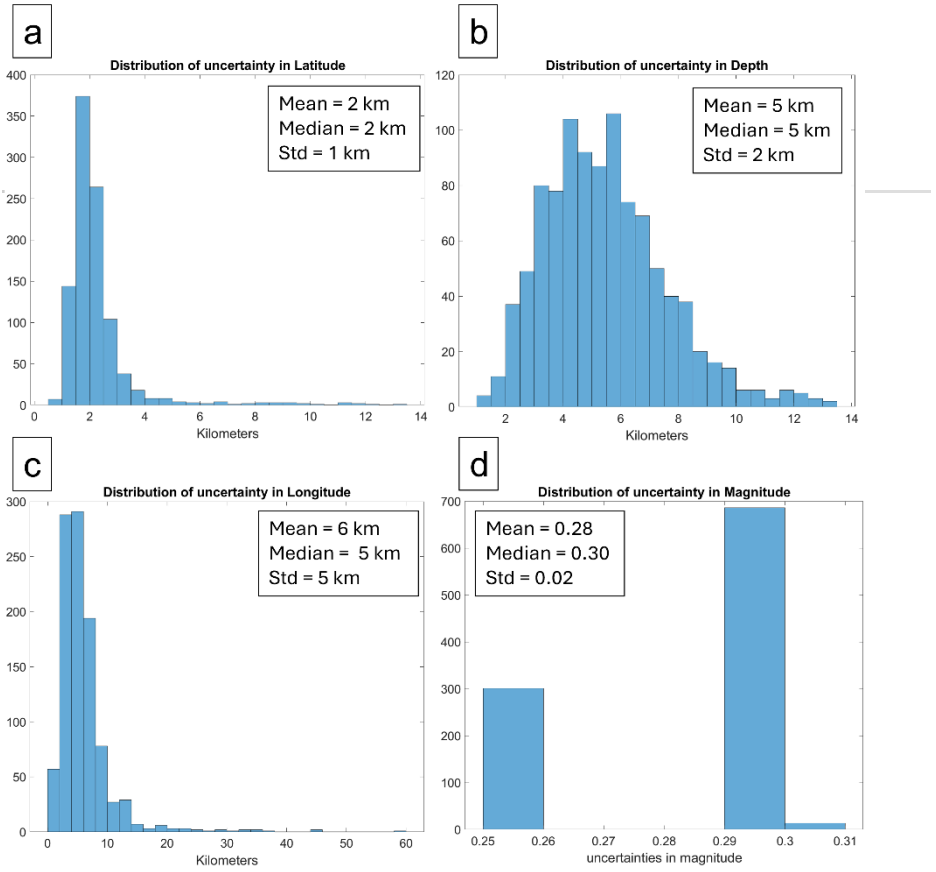

Supplementary Figure S11. In this figure we show the uncertainties distribution for all the parameters estimated by QuakeUp. These distributions were obtained using 1000 different configurations in which just the 30% of the stations in the network works.

4. Maps of the calculated Tsunami Travel Times

The tsunami travel time calculated for the two regions are presented in Supplementary Figure S12. We obtained this figure by considering a 15 arc-sec bathymetric model (SRTM15+) and the shallow water approximation for the tsunami propagation. The fault models presented in the figure as white dashed boxes, were obtained with two different strategies, well explained in the main text. The fault in panel a, relative to the 2020 Aegean Sea event, was obtained starting from the focal mechanism proposed by IPGP[4] and calculating the dimensions with the Wells and Coppersmith scale relationship[5]. In panel b, instead, the fault model shown is the same used to produce the simulated traces and it's the one retrieved by Michelini[6]. These colormaps are useful to quantify the lead-times available at places outside the two blind zones. Let us consider, for instance, the cities of Agios Kirkos and Kusadasi in panel a. These two coastal cities were reached by the tsunami waves in about 15 minutes. The alert provided by Early-Est and the PTF (yellow line) would have been issued in 3 minutes and 40 seconds, resulting in about 11 minutes and 20 seconds of time for the people in those cities to perform mitigation actions. However the alert provided by the combination of QuakeUp and the PTF is issued in 1 minute and 10 seconds (cyan line), providing 13 minutes and 50 seconds of lead-time at the same cities. Similar considerations can be done for the Messina Strait scenario (panel b). Let us consider the city of Catania, which would be reached buìy the tsunami waves in about 15 minutes. Considering that the combination of the estimations provided

by Early-Est and PTF would have issued an alert in 3 minutes and 40 seconds (yellow line), people living in Catania would have had 11 minutes and 20 seconds of lead-time using the current system. The alert provided by the chain formed by QuakeUp and PTF would have been issued in 48 seconds, meaning that the people of Catania would have had 14 minutes and 8 seconds of time to take cover.

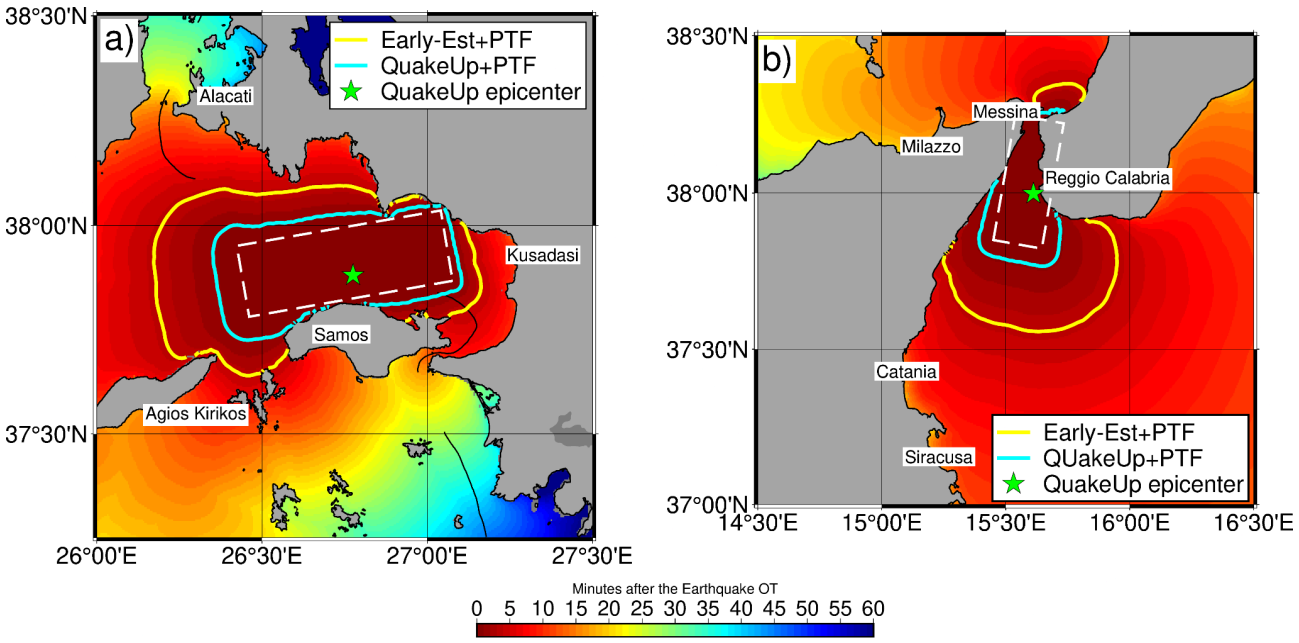

Supplementary Figure S12. Tsunami Travel Times maps. The colormaps in panel a and panel b show the tsunami travel times expressed in minutes calculated, respectively, for the 2020 Aegean Sea event and for the Simulated magnitude 7.0 Messina strait event. The fault models are represented in both panels as a dashed white box, while the epicenters estimated by QuakeUp in the two scenarios are represented as a green star. The cyan shapes on the figure are the blind zones associated with the alert that would have been produced by the combination of QuakeUp and PTF estimations, while the yellow shapes are the blind zones associated with the combination of the estimations produced by Early-Est and the PTF.

5. Hazard curves at any Prediction point

Figure S13 shows all the hazard curves calculated by the PTF at all the prediction points in the region around the epicenter of the Samos earthquake. The blue solid lines are the curves calculated starting from the epicenter estimated by Early-Est, while the dashed lines are the curves calculated using the location estimated by Early-Est. In the lower part of each panel the relative difference is also shown as a function of the waves' height. At every forecast point in the region the differences between the two curves are very little, reaching the maximum value of 0.3. It is worth to notice that no trend can be identified looking at the behaviour of the differences in the hazard curves.

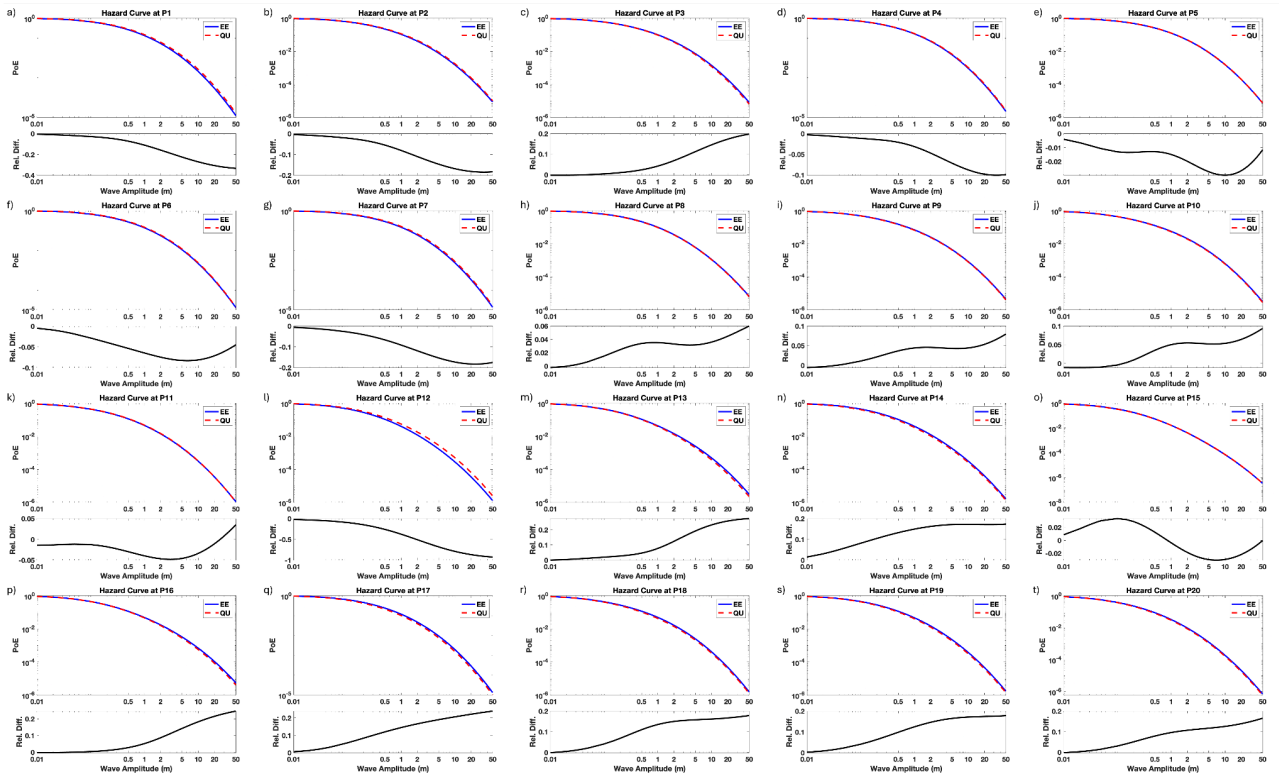

Supplementary Figure S13. Hazard curves for the Samos earthquake. In each panel the blue curve represents the hazard curve calculated using the epicentral position estimated by Early-Est and the dashed red curve represents the hazard curve calculated from the epicenter estimated by QuakeUp. The difference between the two curves is plotted as a black line in the lower part of each panel.

Figure S14 shows the hazard curves calculated for all the prediction points in the Messina Strait region. In each panel the blue line is the curve calculated for the magnitude 7 simulated event and the red dashed line is the curve calculated for the simulated magnitude 6 event. As we expected the difference between the two curves (black line in each panel) increases as the waves' height increase. That's because a magnitude 7 earthquake produces higher tsunami waves than a magnitude 6 earthquake. Looking at the points located further from the epicenter, the difference is remarkable also considering low waves' height. This means that the bigger event produces a tsunami that has an impact on a larger area around the fault.

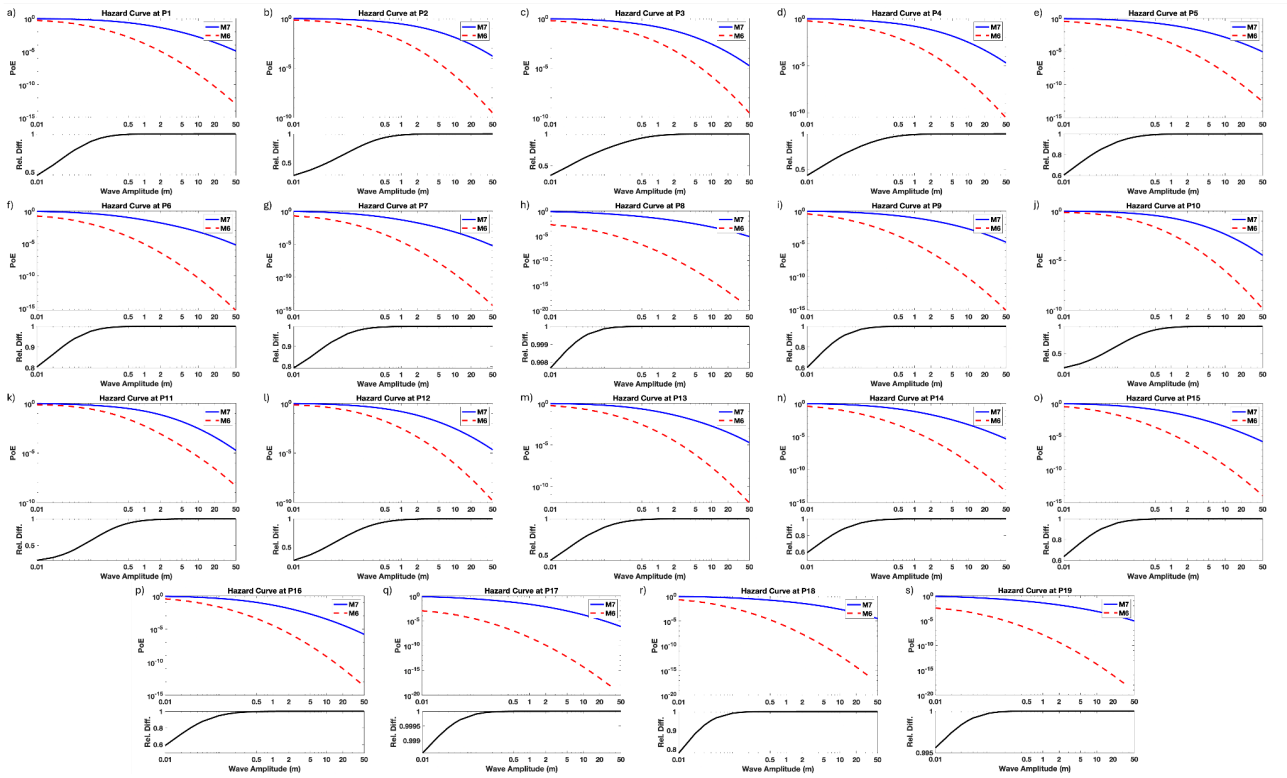

Supplementary Figure S14. Hazard curves for two simulated earthquakes. In each panel the blue curve represents the hazard curve calculated using the epicentral position estimated by QuakeUp for a magnitude 7 simulated event and the dashed red curve represents the hazard curve calculated from the same epicenter for a magnitude 6 simulated earthquake. The difference between the two curves is plotted as a black line in the lower part of each panel.

Supplementary References

[1] "IRIS Bulletin and waveform downloads," https://ds.iris.edu/wilber3/find_event.

[2] S. Akkar, M. A. Sandıkkaya, and J. J. Bommer, "Empirical ground-motion models for point- and extended-source crustal earthquake scenarios in Europe and the Middle East," *Bulletin of Earthquake Engineering*, vol. 12, no. 1, pp. 359–387, Feb. 2014, doi: 10.1007/s10518-013-9461-4.

[3] D. Bindi *et al.*, "Pan-European ground-motion prediction equations for the average horizontal component of PGA, PGV, and 5%-damped PSA at spectral periods up to 3.0 s using the RESORCE dataset," *Bulletin of Earthquake Engineering*, vol. 12, no. 1, pp. 391–430, Feb. 2014, doi: 10.1007/s10518-013-9525-5.

[4] SCARDEC method: Analysis of the earthquake source, Available at:

http://geoscope.ipgp.fr/index.php/en/catalog/earthquake-description?seis=us7000c7y0 (Accessed:

24 April 2025)

[5] Wells, D. L. and Coppersmith, K. J. "New Empirical Relationships among Magnitude, Rupture

Length, Rupture Width, Rupture Area, and Surface Displacement," 1994.

[6] Michelini, A., Lomax, A., Nardi, A., Rossi, A., Palombo, B., & Bono, A. (2005). A modern re-examination of the locations of the 1905 Calabria and the 1908 Messina Straits earthquakes. In *Geophysical Research Abstracts* (Vol. 7, p. 07909).